

This article was downloaded by:

On: 23 January 2011

Access details: *Access Details: Free Access*

Publisher *Taylor & Francis*

Informa Ltd Registered in England and Wales Registered Number: 1072954 Registered office: Mortimer House, 37-41 Mortimer Street, London W1T 3JH, UK



Journal of Coordination Chemistry

Publication details, including instructions for authors and subscription information:

<http://www.informaworld.com/smpp/title~content=t713455674>

Synthesis, characterization, thermal and redox behavior, and biological activity of Ni(II), Cu(II), and Zn(II) complexes containing pyridoxine and imidazole moieties

M. A. Neelakantan^a; M. Sundaram^a; S. Thalamuthu^a; M. Sivasankaran Nair^b

^a Chemistry Research Centre, National Engineering College, Tamil Nadu, India ^b Department of Chemistry, Manonmaniam Sundaranar University, Tirunelveli 627 012, Tamil Nadu, India

First published on: 24 June 2010

To cite this Article Neelakantan, M. A. , Sundaram, M. , Thalamuthu, S. and Nair, M. Sivasankaran(2010) 'Synthesis, characterization, thermal and redox behavior, and biological activity of Ni(II), Cu(II), and Zn(II) complexes containing pyridoxine and imidazole moieties', *Journal of Coordination Chemistry*, 63: 11, 1969 – 1985, First published on: 24 June 2010 (iFirst)

To link to this Article: DOI: 10.1080/00958972.2010.493583

URL: <http://dx.doi.org/10.1080/00958972.2010.493583>

PLEASE SCROLL DOWN FOR ARTICLE

Full terms and conditions of use: <http://www.informaworld.com/terms-and-conditions-of-access.pdf>

This article may be used for research, teaching and private study purposes. Any substantial or systematic reproduction, re-distribution, re-selling, loan or sub-licensing, systematic supply or distribution in any form to anyone is expressly forbidden.

The publisher does not give any warranty express or implied or make any representation that the contents will be complete or accurate or up to date. The accuracy of any instructions, formulae and drug doses should be independently verified with primary sources. The publisher shall not be liable for any loss, actions, claims, proceedings, demand or costs or damages whatsoever or howsoever caused arising directly or indirectly in connection with or arising out of the use of this material.

Synthesis, characterization, thermal and redox behavior, and biological activity of Ni(II), Cu(II), and Zn(II) complexes containing pyridoxine and imidazole moieties

M.A. NEELAKANTAN*†, M. SUNDARAM†, S. THALAMUTHU†
and M. SIVASANKARAN NAIR‡

†Chemistry Research Centre, National Engineering College, K.R. Nagar,
Kovilpatti 628 503, Tamil Nadu, India

‡Department of Chemistry, Manonmaniam Sundaranar University,
Tirunelveli 627 012, Tamil Nadu, India

(Received 15 October 2009; in final form 29 January 2010)

Several mixed ligand complexes $[M(II)(PN)(B)]$ [$M(II) = Ni(II), Cu(II), \text{ and } Zn(II)$] derived from pyridoxine (PN) and imidazoles (B), namely imidazole (him), benzimidazole (bim), histamine (hist), and L-histidine (his), were synthesized. The complexes are characterized by elemental analysis, IR, UV-Vis 1H NMR, and ESR spectroscopy. In $[M(II)(PN)B]$, the monovalent anion of PN is bidentate to $M(II)$ ($-O, -OH$), him, bim monodentate ($-N$), his bidentate ($-N, -N$), and his tridentate ($-O, -N, -N$). Magnetic moment studies showed that the $Ni(II)$ complexes and $Cu(II)$ -PN-his have octahedral configuration while the other $Cu(II)$ complexes have distorted tetrahedral geometry. The $g_{\parallel}/A_{\parallel}$ values calculated from the X-band ESR spectra of $Cu(II)$ complexes in DMSO at 300 and 77 K supports the geometry. The thermal behavior (TG/DTA) of the synthesized complexes indicates the presence of lattice as well as coordinated water in the complexes. The *in vitro* biological activity of the mixed ligand complexes was tested against common bacteria, yeast, and fungi. The results in comparison with the control indicate that most of the complexes exhibit higher biological activities. The oxidative DNA cleavage studies of the mixed ligand complexes were performed using gel electrophoresis.

Keywords: Mixed ligand complexes; Spectral studies; Redox behavior; Antimicrobial activity; DNA cleaving

1. Introduction

Vitamin B6 existing in three forms, namely pyridoxol, pyridoxamine, and pyridoxal, in plants and in the tissues of animals is a very important biodynamic agent. The major forms of vitamin B6 from animal food products are pyridoxal and pyridoxal 5'-phosphate, whereas pyridoxine (PN), pyridoxine-5'-phosphate, pyridoxamine, and pyridoxamine-5'-phosphate are the main forms obtained from plants [1]. The phosphate forms of vitamin B6 in food are dephosphorylated in the intestinal lumen and PN, pyridoxal, and pyridoxamine are taken up from the small intestine by an

*Corresponding author. Email: maneels@rediffmail.com

energy-dependent process. All three forms of vitamin B6 are converted into pyridoxal-5'-phosphate in the tissues which exerts anti-proliferative and anti-tumoral activities [2, 3]. The importance of metallic ions in some enzymatic processes involving vitamin B6 derivatives as cofactors is well established [4, 5]. PN was the first isolated vitamin B6 and is essential in the diet for the metabolism of amino acids and the maintenance of body cells [6]. Binding of PN occurs primarily through the chelation of phenolic and 4'-hydroxy methyl groups [7–9]. Bonding through other ligand sites has been suggested in solution [10]. Imidazole is an important constituent of many biological compounds and an active site of many enzymes [11], acting as a proton donor/acceptor and charge transfer agent ligated to metal ions in B12 coenzymes.

This article reports the synthesis and characterization of some mixed ligand complexes of Ni(II), Cu(II), and Zn(II) containing PN and imidazole moieties, namely imidazole (him), benzimidazole (bim), histamine (hist) and L-histidine (his) (figure S1). Thermal behavior of these complexes were studied. The *in vitro* activity of the synthesized complexes against common bacteria, yeast, and fungi has been carried out. Oxidative DNA cleavage of mixed ligand complexes were performed using gel electrophoresis.

2. Experimental

2.1. Materials and instrumentation

All chemicals and solvents used for synthesis were of reagent grade. PN, imidazole (him), benzimidazole (bim), histamine (hist), and L-histidine (his) were purchased from Aldrich and used without purification. All other reagents and metal chlorides were procured from commercial sources. Doubly distilled water was used in the preparation of all the solutions. Solvents used for spectroscopic studies were purified and dried by standard procedures [12]. Elemental analyses were performed using a Thermo Finnigan Flash EA 1112 CHNS analyzer. Infrared (IR) spectra were recorded with samples as KBr pellets with a Shimadzu FTIR – 8400S spectrophotometer. UV-Vis spectra were obtained on a JASCO-530 spectrophotometer. ^1H NMR spectra were recorded on a Bruker AMX 400 MHz spectrometer using TMS as reference in DMSO. The X-band ESR spectra of Cu(II) complexes in DMSO at room temperature and liquid nitrogen temperature were recorded on a Varian E112 spectrophotometer using diphenylpicrylhydrazyl (DPPH) as internal standard. Thermogravimetric analyses were measured from room temperature to 1000°C at a heating rate of 20°C min⁻¹ using a Perkin Elmer Diamond TG/DTA instrument. Conductance values of the complexes were obtained on a Systronics Model-611 digital conductivity meter using DMSO as solvent. Magnetic susceptibility measurements were carried out for solid complexes using a Guoy balance at 302 ± 2 K.

2.2. Synthesis

2.2.1. Synthesis of Cu(II)–PN–him (I). Ethanolic solution (10 cm³) of CuCl₂·2H₂O (0.1705 g, 1.0 mmol) was stirred and ethanolic solutions (10 cm³) of PN (0.1692 g, 1.0 mmol) and (10 cm³) him (0.068 g, 1.0 mmol) were added dropwise at

room temperature. After the slow addition of ligands was completed, the mixture was refluxed for 8 h with constant stirring. The dirty green compound (**1**) was collected by filtration and washed several times with ethanol and finally with diethyl ether until the washings become colorless. The products were dried in air and stored in a desiccator over anhydrous calcium chloride under vacuum. Anal. Calcd for $[\text{CuC}_{11}\text{H}_{16}\text{O}_4\text{N}_3]\text{Cl}$ (%): C, 37.39; H, 4.50; N, 11.89; Cu, 18.00. Found (%): C, 37.36; H, 4.46; N, 11.81; Cu, 17.95. Color, dirty green; m. 285°C; Yield, 64%; Λ_m , 35 mho mol⁻¹ cm².

2.2.2. Synthesis of 2–12. The other mixed ligand complexes were synthesized in an identical manner as described for the synthesis of **1**.

(*Cu(II)*–*PN*–*bim*) (**2**): Anal. Calcd for $[\text{CuC}_{15}\text{H}_{18}\text{O}_4\text{N}_3]\text{Cl}$ (%): C, 44.67; H, 4.47; N, 10.42; Cu, 15.77. Found (%): C, 44.62; H, 4.39; N, 10.37; Cu, 16.12; Color, Green; m. 254°C; Yield, 62%; Λ_m , 30 mho mol⁻¹ cm².

(*Cu(II)*–*PN*–*hist*) (**3**): Anal. Calcd for $[\text{CuC}_{13}\text{H}_{19}\text{O}_3\text{N}_4]\text{Cl}$ (%): C, 41.27; H, 5.03; N, 14.81; Cu, 16.81. Found (%): C, 41.32; H, 4.99; N, 13.98; Cu, 16.83; Color, Green; m. 269°C; Yield, 61%; Λ_m , 28 mho mol⁻¹ cm².

(*Cu(II)*–*PN*–*his*) (**4**): Anal. Calcd for $[\text{CuC}_{14}\text{H}_{20}\text{O}_6\text{N}_4]$ (%): C, 41.63; H, 4.96; N, 13.88; Cu, 15.75. Found (%): C, 41.60; H, 4.98; N, 13.82; Cu, 15.85. Color, Green; m. 290°C; Yield, 62%; Λ_m , 10 mho mol⁻¹ cm².

(*Ni(II)*–*PN*–*him*) (**5**): Anal. Calcd for $[\text{NiC}_{11}\text{H}_{20}\text{O}_6\text{N}_3]\text{Cl}$ (%): C, 34.38; H, 5.20; N, 10.93; Ni, 15.28. Found (%): C, 34.43; H, 5.17; N, 11.02; Ni, 15.21; Color, Pale green; m. 245°C; Yield, 64%; Λ_m , 32 mho mol⁻¹ cm².

(*Ni(II)*–*PN*–*bim*) (**6**): Anal. Calcd for $[\text{NiC}_{15}\text{H}_{22}\text{O}_6\text{N}_3]\text{Cl}$ (%): C, 41.46; H, 5.07; N, 9.67; Ni, 13.52. Found (%): C, 41.42; H, 5.04; N, 9.70; Ni, 13.55; Color, Pale green; m. 215°C; Yield, 60%; Λ_m , 38 mho mol⁻¹ cm².

(*Ni(II)*–*PN*–*hist*) (**7**): Anal. Calcd for $[\text{NiC}_{13}\text{H}_{23}\text{O}_5\text{N}_4]\text{Cl}$ (%): C, 38.13; H, 5.62; N, 13.69; Ni, 14.35. Found (%): C, 38.16; H, 5.58; N, 13.66; Ni, 14.38; Color, Bluish green; m. 230°C; Yield, 62%; Λ_m , 30 mho mol⁻¹ cm².

(*Ni(II)*–*PN*–*his*) (**8**): Anal. Calcd for $[\text{NiC}_{14}\text{H}_{20}\text{O}_6\text{N}_4]$ (%): C, 42.14; H, 5.02; N, 14.05; Ni, 14.72. Found (%): C, 42.16; H, 4.99; N, 14.08; Ni, 14.69; Color, Bluish green; m. 238°C; Yield, 59%; Λ_m , 08 mho mol⁻¹ cm².

(*Zn(II)*–*PN*–*him*) (**9**): Anal. Calcd for $[\text{ZnC}_{11}\text{H}_{16}\text{O}_4\text{N}_3]\text{Cl}$ (%): C, 37.17; H, 4.50; N, 11.83; Zn, 18.50. Found (%): C, 37.12; H, 4.46; N, 11.88; Zn, 18.56; Color, White; m. 280°C; Yield, 63%; Λ_m , 39 mho mol⁻¹ cm².

(*Zn(II)*–*PN*–*bim*) (**10**): Anal. Calcd for $[\text{ZnC}_{15}\text{H}_{18}\text{O}_4\text{N}_3]\text{Cl}$ (%): C, 44.43; H, 4.44; N, 10.37; Zn, 16.22. Found (%): C, 44.39; H, 4.46; N, 10.35; Zn, 16.19; Color, White; m. 250°C; Yield, 60%; Λ_m , 32 mho mol⁻¹ cm².

(*Zn(II)*–*PN*–*hist*) (**11**): Anal. Calcd for $[\text{ZnC}_{13}\text{H}_{19}\text{O}_3\text{N}_4]\text{Cl}$ (%): C, 41.03; H, 4.99; N, 14.73; Zn, 17.28. Found (%): C, 41.00; H, 4.95; N, 14.75; Zn, 17.33; Color, White; m. 225°C; Yield, 65%; Λ_m , 31 mho mol⁻¹ cm².

(Zn(II)-PN-his) (**12**): Anal. Calcd for $[\text{ZnC}_{14}\text{H}_{20}\text{O}_6\text{N}_4]$ (%): C, 41.41; H, 4.93; N, 13.80; Zn, 16.19. Found (%): C, 41.38; H, 4.97; N, 13.76; Zn, 16.23; Color, White; m. 298°C; Yield, 61%; Λ_m , 13 mho mol⁻¹ cm².

2.3. Antimicrobial activity measurement

The *in vitro* activities of **1–12** were tested against the gram positive bacterium (*Staphylococcus aureus*) and the gram-negative bacteria (*Pseudomonas aeruginosa*, *Escherichia coli*, *Proteus species*, *Klebsiella species*), fungus (*Aspergillus niger*), and yeast (*Candida species*) by a modified disc diffusion method [13]. The bacterial subcultures were autoclaved for 20 min at 121°C and at 15 lb pressure before inoculation. The bacteria were then cultured for 24 h at 37°C in an incubator. The test solutions of **1–12** [3×10^{-3} mol L⁻¹ concentration] in aqueous solution were added dropwise to a 10 mm diameter Whatman No. 1 filter paper disc placed at the center of each agar plate. These discs were then kept at 5°C for 1 h and transferred to an incubator maintained at 37°C. After 4 days, the inhibition zone around the discs in each plate was measured. Commercially available ampicillin was used for antibacterial control, while nystatin was used as antifungal control.

2.4. General procedure for DNA cleavage

Gel electrophoresis experiments were performed using CT DNA in 50 mmol L⁻¹ Tris-HCl buffer (pH 7.2) containing 18 mmol L⁻¹ NaCl. The reaction mixture was prepared in the following ways: (1) reaction mixture containing 15 μL of CT DNA, 5 μL of metal complex in DMSO and 4 μL of 7 mmol L⁻¹ H₂O₂ in 28 μL of 50 mmol L⁻¹ Tris-HCl buffer (pH 7.2), (2) 4 μL of 7 mmol L⁻¹ H₂O₂ and 4 μL of 7 mmol L⁻¹ ascorbic acid were added to a mixture of 20 μL of CT DNA (0.05 $\mu\text{g } \mu\text{L}^{-1}$) and 6 μL of 300 $\mu\text{mol L}^{-1}$ metal complex followed by dilution with Tris-HCl buffer (pH 7.2) to a total volume of 40 μL . The reactions were performed after incubating the reaction mixture at 25°C for 2 h in the presence and/or absence of the complexes. The samples were electrophoresed for 2 h at 50 V on 1% agarose gel using tris-HCl buffer, pH 7.2. After electrophoresis, the gel was stained using 1 $\mu\text{g cm}^{-3}$ ethidium bromide (EB) and photographed under UV light.

3. Results and discussion

The complexes are non-hygroscopic solids, stable in air, and soluble in DMF and DMSO. Elemental analyses confirm the proposed formula, M(PN)B (where M(II) = Ni(II), Cu(II), and Zn(II); B = him, bim, hist, and his) (figure S2). The molar conductance values of complexes containing his (**4**, **8**, and **12**) are low in DMSO, indicating the non-electrolytic nature, while the other complexes fall in the expected range of 1 : 1 electrolytes [14].

3.1. Infrared spectra

IR spectrum of PN shows a strong band at 1564 cm^{-1} from $\text{HC}=\text{N}$ ring stretching and does not change in all the complexes, clearly indicating that the pyridine nitrogen of PN is not complexed. PN shows a medium band at 1352 cm^{-1} corresponding to in-plane OH bending of phenol and becomes sharp and shifts to higher frequency in spectra of the complexes [15], indicating the coordination of PN through phenolic oxygen. The phenolic C–O stretch in PN at 1222 cm^{-1} shifts to $1290\text{--}1274\text{ cm}^{-1}$ in the complexes, supporting the coordination of phenolic C–O with the metal. Two bands attributed to alcoholic C–O stretch in spectra of the complexes (one band at $\sim 1020\text{ cm}^{-1}$ and another at $1088\text{--}1070\text{ cm}^{-1}$) indicate one hydroxy methyl coordinates to the metal ion. IR spectra of all complexes show a broad band at $3427\text{--}3020\text{ cm}^{-1}$, assigned to the alcoholic OH stretch of PN, merged with OH stretch of water. From the band at 950 cm^{-1} , water is coordinated in all the complexes except hist complexes for which the absence of coordinated water is confirmed from the absence of rocking, twisting, and wagging vibrational modes at $970\text{--}930$ and $660\text{--}600\text{ cm}^{-1}$. The imidazole containing ligands exhibit a strong imidazole C=N ring band at $1590\text{--}1577\text{ cm}^{-1}$ which is shifted to $1545\text{--}1516\text{ cm}^{-1}$ in all the complexes, indicating the coordination of imidazole nitrogen in the complexes. The IR spectra of hist and his show in-plane deformation δ_{NH} at 1637 and 1622 cm^{-1} , respectively, which shift to $\sim 1590\text{ cm}^{-1}$ in the complexes, indicating the presence of amino of hist and his coordinates (table 1). This is further confirmed by the negative shift of C–N stretch in hist and his complexes [16]. IR spectra of his complexes (**4**, **8**, and **12**) show two bands at $1597\text{--}1574$ and $1394\text{--}1389\text{ cm}^{-1}$, assigned to $\nu(\text{COO}^-)_{\text{asym}}$ and $\nu(\text{COO}^-)_{\text{sym}}$ of carboxylate. The separation between these two vibrations ($200\text{--}347\text{ cm}^{-1}$) suggests unidentate carboxylate. New bands not present in spectra of the free ligands in the range $540\text{--}520$ and $490\text{--}480\text{ cm}^{-1}$ in the spectra of the complexes [17] are attributed to $\nu_{(\text{M}-\text{N})}$ and $\nu_{(\text{M}-\text{O})}$, respectively. The appearance of $\nu_{(\text{M}-\text{N})}$ and $\nu_{(\text{M}-\text{O})}$ supports the involvement of nitrogen and oxygen in complexation.

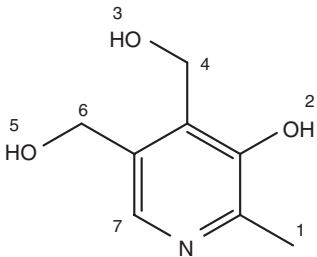
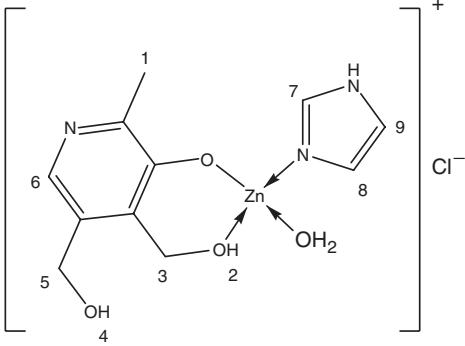
3.2. $^1\text{H-NMR}$ data

The $^1\text{H-NMR}$ spectrum of PN shows a peak at 8.01 ppm assignable to pyridine ring $\text{CH}=\text{N}$ which does not change in the complexes, indicating the non-involvement of pyridine in coordination. PN shows peaks at 2.50, 4.95, and 4.92 ppm, which are assignable to methyl and hydroxy methyl H4 and H6, respectively. In the Zn(II) complexes, upfield shift of H4 is larger than H6 (table 2), suggesting that the oxygen of hydroxymethyl at carbon four is coordinated to Zn(II) [18]. The zinc complexes show a peak (7.88–7.92 ppm) due to imidazole ring $\text{CH}=\text{N}$ downfield shifted from free ligands (**B**) (7.62–7.68 ppm). The remaining signals of imidazole do not change in the Zn(II)–PN–him/bim complexes (figure 1), indicating that him/bim are coordinated to Zn(II) through the imidazole nitrogen only. The α -proton of free his shows a multiple at 3.95 ppm which shifts to 4.23 ppm in the Zn(II)–PN–his complex. This shift is larger than that of Zn(II)–PN–hist, indicating his coordinates Zn(II) through the carboxylate oxygen, amino, and imidazole nitrogens, whereas only amino and imidazole nitrogens are involved during complexation in the case of hist.

Table 1. IR spectral data of PN and M(II)-PN-him/bim/hist/his (1-12) (cm^{-1}).

S. No.	Complex	$\nu(\text{O-H})$	$\nu(\text{C}\equiv\text{N})$	Phenolic $\delta(\text{O-H})$	Phenolic $\nu(\text{C-O})$	Alcoholic $\nu(\text{C-O})$	$\nu(\text{C-N})$	$\delta(\text{N-H})$	$\nu(\text{M-N})$	$\nu(\text{M-O})$
1	PN	3350-3276	1564	1352(m)	1222	1022	-	-	-	-
2	Cu(II)-PN-him	3430-3100	1559 1541	1419(s)	1278	1018 1066	-	-	528	487
3	Cu(II)-PN-bim	3430-3100	1516	1416(s)	1277	1012 1087	-	-	531	485
4	Cu(II)-PN-hist	3430-3100	1556 1545	1408(s)	1275	1018 1085	1048	1590	532	479
5	Cu(II)-PN-his	3430-3100	1567	1394(s)	1279	1020	1035	1589	541	465
6	Ni(II)-PN-him	3430-3100	1560 1541	1418(s)	1292	1016 1070	-	-	525	475
7	Ni(II)-PN-bim	3430-3100	1561 1527	1415(s)	1289	1017 1076	-	-	521	479
8	Ni(II)-PN-hist	3430-3100	1552 1535	1420(s)	1278	1019 1080	1050	1584	529	476
9	Ni(II)-PN-his	3430-3100	1557	1422(s)	1282	1016	1037	1592	530	480
10	Zn(II)-PN-him	3430-3100	1554 1538	1416(s)	1276	1019 1085	-	-	535	469
11	Zn(II)-PN-bim	3430-3100	1536	1419(s)	1279	1021 1069	-	-	532	482
12	Zn(II)-PN-hist	3430-3100	1552 1532	1425(s)	1285	1017 1070	1047	1591	536	480
13	Zn(II)-PN-his	3430-3100	1568 1539	1423(s)	1280	1018 1082	1032	1595	531	477

Table 2. $^1\text{H-NMR}$ spectral data of the PN and **9** (ppm).

	Protons	Chemical shift (ppm)
 <p>PN</p>	H1	2.62
	H2	–
	H3	–
	H4	4.95
	H5	–
	H6	4.92
	H7	8.01
 <p>Zn(II)-PN-him</p>	H1	2.44
	H2	–
	H3	4.45
	H4	–
	H5	4.90
	H6	7.95
	H7	8.48
	H8	7.43
	H9	7.04

3.3. Electronic absorption spectra and magnetic studies

Electronic spectra of free ligands and their Ni(II) and Cu(II) complexes were recorded at room temperature in DMSO (figure S3). The λ_{max} of PN is at 284 nm from $\pi-\pi^*$ transition of pyridine C=N. This band does not change in spectra of complexes suggesting that the pyridine of PN does not complex. The imidazole containing ligands show two bands at 250–270 and 290–345 nm, attributable to $\pi-\pi^*$ and $n-\pi^*$ of imidazole C=N, respectively. These bands shift to longer wavelength in the complexes suggesting that imidazole nitrogen coordinates. The electronic spectra of Cu(II)–PN–him/bim/hist show one intense band at 350–420 nm (table 3) due to charge transfer from ligand to metal. Electronic spectra of Cu(II)–PN–him shows a less intense d–d band at 829 nm [19, 20] while Cu(II)–PN–bim shows a band at 875 nm. The higher value compared to him complex can be explained on the basis of the bulkiness of bim which leads to slight distortion. The electronic spectrum of Cu(II)–PN–hist exhibits a band at 840 nm due to d–d transition. This indicates that these complexes have distorted tetrahedral geometry. The electronic spectrum of Cu(II)–PN–his shows octahedral environment with a band at 703 nm which can be assigned to $^2E_g \rightarrow ^2T_{2g}$ transition. The μ_{eff} values were found to be 1.95, 1.98, 1.96, and 1.88 BM for complexes

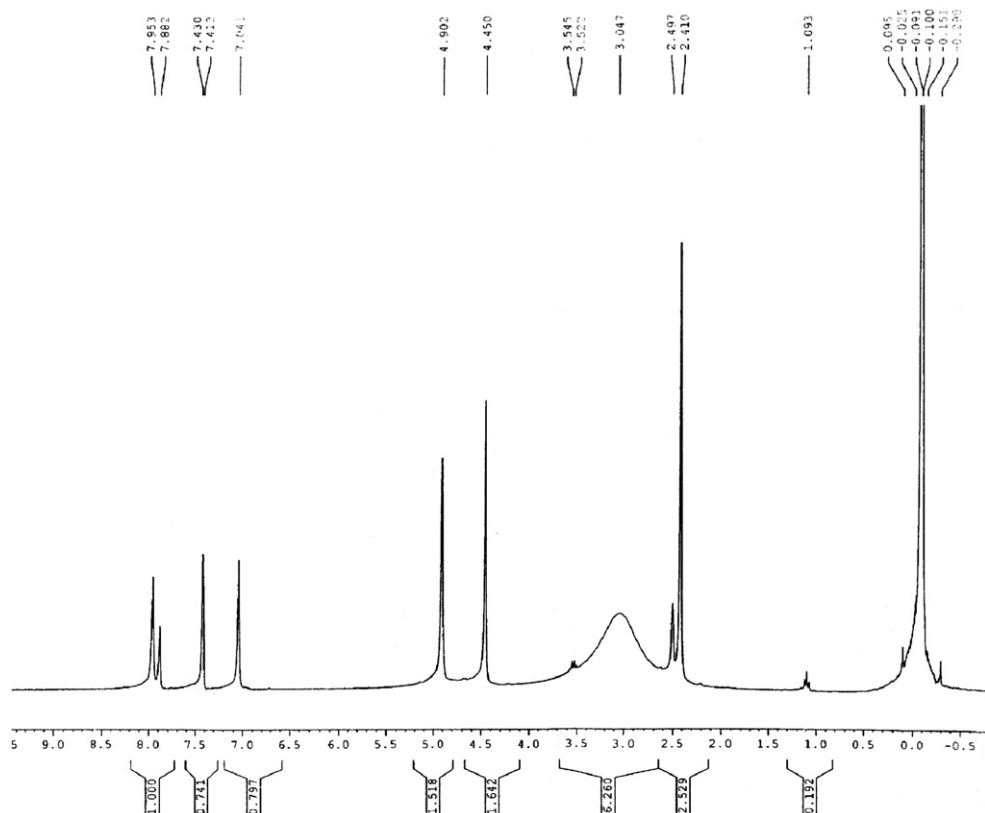


Figure 1. $^1\text{H-NMR}$ spectrum of Zn(II)-PN-him (9).

1, 2, 3, and 4, respectively, which are well within the expected region (1.92–2.00 BM) found for Cu(II) complexes. The higher magnetic moments of copper complexes than the spin only value (1.73 BM) imply the presence of a low-lying excited term, which is able to mix some of its orbital angular momentum with spin angular momentum of the ground state. The electronic spectra of all the greenish Ni complexes show octahedral environment with a band at 1000 nm assigned to $^3\text{A}_{2g} \rightarrow ^3\text{T}_{2g}$ (F). In addition, a multiple structured band in the range of 650–790 nm is observed which is assignable to $^3\text{A}_{2g} \rightarrow ^3\text{T}_{1g}$ (F) transition. The multiple structures arise due to the spin forbidden transitions of $^1\text{E}_g$ state which lies so close to $^3\text{T}_{1g}$ due to extensive mixing. The third band is in the range of 410–430 nm due to $^3\text{A}_{2g} \rightarrow ^3\text{T}_{1g}$ (P) transition [19]. The observed magnetic moment value in the range of 3.15–3.22 BM also supports the octahedral geometry for all nickel complexes.

3.4. ESR spectra of Cu(II) complexes 1–4

The extent of distortion from planarity of these complexes has been studied by ESR measurements (figure 2) in DMSO performed for all the Cu(II) complexes. The spectrum at 300 K shows an isotropic pattern due to tumbling motion of

Table 3. Electronic absorption spectral data of complexes of Ni(II) and Cu(II)-PN-imidazole containing ligands (1-8).

S. No.	Complex	λ_{\max} (cm ⁻¹)	Band assignments	Geometry	μ_{eff} (BM)
1	Cu(II)-PN-him	283, 383 829	INCT d-d envelope	Distorted Tetrahedral	1.95
2	Cu(II)-PN-bim	278, 419 875	INCT d-d envelope	Distorted Tetrahedral	1.98
3	Cu(II)-PN-hist	285, 405 890	INCT d-d envelope	Distorted Tetrahedral	1.96
4	Cu(II)-PN-his	284, 348 703	INCT $^2E_g \rightarrow ^2T_{2g}$	Distorted Octahedral	1.88
5	Ni(II)-PN-him	258, 284 410 692 1018	INCT $^3A_{2g} \rightarrow ^3T_{1g}(P)$ $^3A_{2g} \rightarrow ^3T_{1g}(F)$ $^3A_{2g} \rightarrow ^3T_{2g}(F)$	Distorted Octahedral	3.18
6	Ni(II)-PN-bim	284, 334 419 699 1072	INCT $^3A_{2g} \rightarrow ^3T_{1g}(P)$ $^3A_{2g} \rightarrow ^3T_{1g}(F)$ $^3A_{2g} \rightarrow ^3T_{2g}(F)$	Distorted Octahedral	3.22
7	Ni(II)-PN-hist	295, 380 425 680 1069	INCT $^3A_{2g} \rightarrow ^3T_{1g}(P)$ $^3A_{2g} \rightarrow ^3T_{1g}(F)$ $^3A_{2g} \rightarrow ^3T_{2g}(F)$	Distorted Octahedral	3.20
8	Ni(II)-PN-his	258, 285 430 648 1058	INCT $^3A_{2g} \rightarrow ^3T_{1g}(P)$ $^3A_{2g} \rightarrow ^3T_{1g}(F)$ $^3A_{2g} \rightarrow ^3T_{2g}(F)$	Distorted Octahedral	3.15

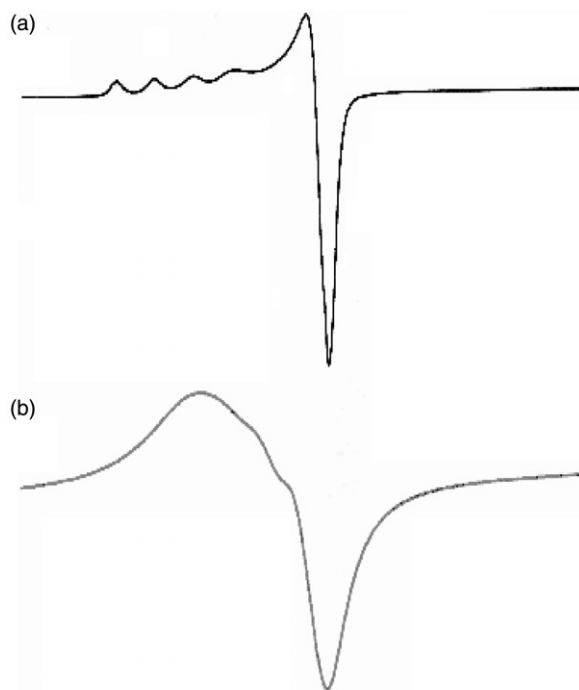


Figure 2. ESR spectra of Cu(II)-PN-him (I) in DMSO at 77 (a) and 300 K (b).

the molecules. But, the spectrum for the frozen solution shows anisotropic pattern for the powder sample, i.e., four well-resolved peaks of low intensities in the low-field region and one intense peak in the high-field region resulting from the coupling of the unpaired electron with the nuclear spin of Cu(II). The ESR spectra of **1–4** exhibit axially symmetric g -tensor parameters with $g_{\parallel} > g_{\perp} > 2.0023$, indicating that the copper site has a $d_{x^2-y^2}$ ground state characteristic of tetrahedral, square-planar or octahedral stereochemistry (table 4). All the copper complexes have g_{\parallel} and g_{\perp} values in the range of 2.25–2.38 and 2.04–2.06, respectively. Massacesi *et al.* [21, 22] reported that g_{\parallel} values are in the range 2.3–2.4 for complexes containing copper–oxygen bonds and 2.2–2.3 for copper–nitrogen bonds. The present copper complexes have g_{\parallel} =2.25–2.38 in conformity with both Cu–O and Cu–N bonds in the mixed ligand copper complexes. The calculated g_{av} from the relation $g_{av}=1/3 (g_{\parallel} + 2g_{\perp})$ is in the range of 2.11–2.18. The deviation from that of the free electron value (2.0023) is due to covalence and provides further support for tetrahedral-distorted symmetry associated with $d_{x^2-y^2}$ rather than d_{z^2} [23]. G values were in the range of 5–6 for all the complexes, indicating no Cu–Cu interaction [24], confirmed by no band corresponding to $M_s = \pm 2$ transition observed in spectra. The A_{\parallel} values are in the range of $130\text{--}137 \times 10^{-4} \text{ cm}^{-1}$ for Cu(II)-PN-him/bim/hist complexes, comparable to distorted tetrahedral arrangement around copper. For Cu(II)-PN-his complex, a value of $145 \times 10^{-4} \text{ cm}^{-1}$ is comparable to distorted octahedral arrangement around copper. The lowering of A_{\parallel} values of the complexes is in the order $\text{him} > \text{hist} > \text{bim}$, probably an indication of distortion of the copper environment. These reduced A_{\parallel} values in tetrahedral symmetry are explained by

Table 4. The spin Hamiltonian parameters of 1–4 in DMSO at 300 and 77 K.

Complex	Hyperfine constant $\times 10^{-4}$ (cm $^{-1}$)													
	K_{\parallel}	K_{\perp}	K	g_{iso}	α	A_{\parallel}	A_{\perp}	g_{\parallel}	g_{\perp}	g_{avg}	α^2	β^2	γ^2	$g_{\parallel}/A_{\parallel}$
Cu(II)–PN–him	0.49	0.28	0.45	2.09	0.67	136	82	2.26	2.04	2.11	0.44	1.1	0.64	165
Cu(II)–PN–bim	0.53	0.38	0.45	2.12	0.66	134	73	2.29	2.05	2.13	0.43	1.23	0.82	170
Cu(II)–PN–hist	0.47	0.28	0.43	2.07	0.65	135	74	2.25	2.04	2.11	0.45	0.89	0.71	166
Cu(II)–PN–his	0.43	0.25	0.46	2.10	0.72	135	76	2.24	2.06	2.12	0.62	0.95	0.66	126

4s and 4p orbitals in the ground state mixing in low symmetry complexes. The distortion from the plane increases with increasing g_{\parallel} values and decreasing A_{\parallel} values. So, the value of $g_{\parallel}/A_{\parallel}$ ratio is a good criterion to determine the distortion level [25]. The values of $g_{\parallel}/A_{\parallel}$ are 165 cm $^{-1}$, 170 cm $^{-1}$, and 166 cm $^{-1}$ for Cu(II)–PN–him, Cu(II)–PN–bim, and Cu(II)–PN–hist, respectively, indicating slight distortion in the tetrahedral arrangement around Cu(II).

3.5. Thermogravimetric studies

TGA/DTA show good agreement with the formulas suggested from the analytical data. The complexes show gradual loss in weight due to decomposition by fragmentation with increasing temperature. The thermogram of Cu(II)/Zn(II)–PN–him/bim complexes show weight loss corresponding to a coordinated water at 150–200, whereas in Ni(II) complexes weight loss corresponds to three coordinated waters. In the second step, the weight loss is for chloride up to 310°C. The third step from 280 to 550°C corresponds to the loss of him/bim in the complexes. The thermogram shows weight loss corresponding to the decomposition of PN at 560–840°C. The final metallic oxide is confirmed by IR spectral data and expected weight loss measurements. For M(II)–PN–hist there is no weight loss from 70°C to 200°C, indicating the absence of coordinated and lattice water in the compound. The remaining fragmentations are similar to the decomposition of him/bim complexes. In the thermogram of his complexes, after the loss of one water molecule, his decomposes in multi steps in the temperature region 300–623°C with the elimination of CO $_2$. For Cu(II)–PN–him complex, the decomposition process (figure S4) is given in scheme S1.

3.6. Cyclic voltammetry

The cyclic voltammetric behavior of PN and Cu(II)–PN–him/bim/hist/his complexes (0.003 mol L $^{-1}$) were studied at glassy carbon (GC), Pt and Ag electrodes in DMSO in the presence of 0.05 mol L $^{-1}$ [Bu $_4$ N]ClO $_4$ solution as supporting electrolyte with scan rate of 25–100 mV s $^{-1}$. The electrochemical oxidation and reduction potentials were measured with respect to Ag/AgCl/KCl (satur.) and are given in table S1. Figure 3 shows the voltammogram of Cu(II) complexes at different scan rates. The ligand PN displays waves at E_{pc} (–0.906 V) and E_{pa} (0.532 V) with the scan rate of 100 mV s $^{-1}$. As the scan rate increases from 25 to 100 mV s $^{-1}$, the cathodic and anodic peak separation (ΔE_{p}) increases, indicating the reversibility of the process. The anodic and cathodic

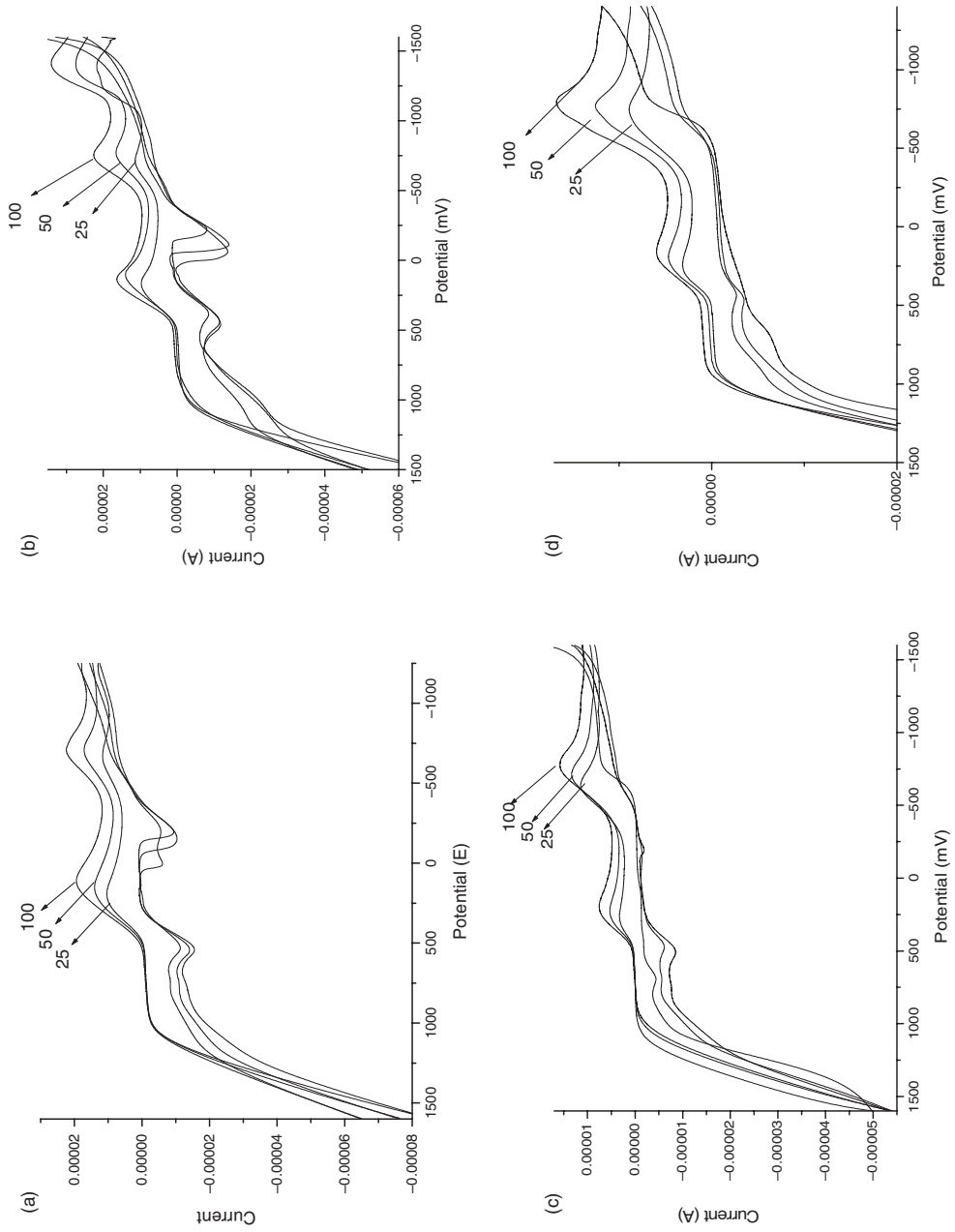


Figure 3. Cyclic voltammograms of 1-4.

peaks of the free ligand disappear in voltammograms of all the metal complexes, indicating coordination with Cu(II). All the complexes show well-defined waves in cathodic and anodic regions. The cyclic voltammogram of Cu(II)–PN shows two cathodic peaks, one in the positive region [Cu(III) → Cu(II)] and another in the negative potential region [Cu(II) → Cu(I)]. The corresponding two anodic peaks are observed at 0.547 V [Cu(II) → Cu(III)] and –0.195 V [Cu(I) → Cu(II)]. As the scan rate increases from 25 to 100 mV s^{–1}, first cathodic peak is shifted to negative potential and its corresponding anodic peak is shifted to positive potential and the I_{pa}/I_{pc} values are approximately one, clearly demonstrates that the Cu(III)/Cu(II) process is irreversible one electron transfer. The cyclic voltammograms of Cu(II)–PN–him/bim/hist/his complexes are quite different from Cu(II) to PN complex. In Cu(II)–PN–him/bim/hist/his complexes, the cathodic peaks are shifted to more negative potentials indicating the formation of mixed ligand complexes. Cu(II)–PN–him shows two redox waves, one in the positive potential region ($E_{pc1}=0.142$ V, $E_{pa1}=0.376$ V) and another in the negative potential region ($E_{pc2}=-0.174$, $E_{pa2}=-0.210$ V) with an additional cathodic peak at –1.391 V [Cu(I) → Cu(0)]. The I_{pa}/I_{pc} value of the redox wave in the negative potential region is greater than 1.5, showing that the anodic peak at –0.210 V is a two-electron process [Cu(0) → Cu(II)]. The peak separation between the anodic and cathodic potential is larger and increases with increasing scan rate from 25 to 100 mV s^{–1}, indicating irreversible process. The Cu(II)–PN–bim/hist/his complexes give two cathodic peaks with the scan rates 25, 50, and 100 mV s^{–1}. In the reverse scan, Cu(II)–PN–bim complex gives two anodic peaks, whereas Cu(II)–PN–hist/his complexes give only one anodic peak in the positive potential region. The peak corresponding to Cu(I) → Cu(II) is not observed showing that Cu(I) is stabilized by hist and his. At lower scan rate (25 mV s^{–1}), Cu(II)–PN–bim gives one oxidation peak in the positive potential region (0.687 V) due to Cu(II) → Cu(III) and the peak from Cu(I) → Cu(II) is not observed, suggesting that Cu(I) is stabilized by bim. The ΔE_p of Cu(III)/Cu(II) is larger and increases with increasing the scan rate, revealing uncompensated resistance effect [26] and irreversible process.

3.7. Scanning electron micrograph

The morphology and particle size of the complexes are obtained from scanning electron micrograph (SEM). Figure 4 depicts the SEM photograph of the complexes. From the pictograph, the uniform matrix and homogeneity of the material is clearly revealed. Layer morphologies with particle size in the range 10–12 μm are observed for **1–12**.

3.8. Antimicrobial activity

The metal complexes **1–12** were tested for their inhibitory effects on the growth of gram positive (*S. aureus*) and gram negative bacteria (*P. aeruginosa*, *E. coli*, *P. species*, *K. species*), fungus (*A. niger*), and yeast (*C. species*) by a modified disc diffusion method (table 5). The standard drugs ampicillin and nystatin were also tested for their antibacterial and antifungal activity at the same concentration under the conditions to that of the test compounds. From the results, it is clear that the inhibition zone of mixed ligand complexes is higher than those of the control and the binary complexes. It is difficult to compare these results for the antimicrobial activities with those reported by

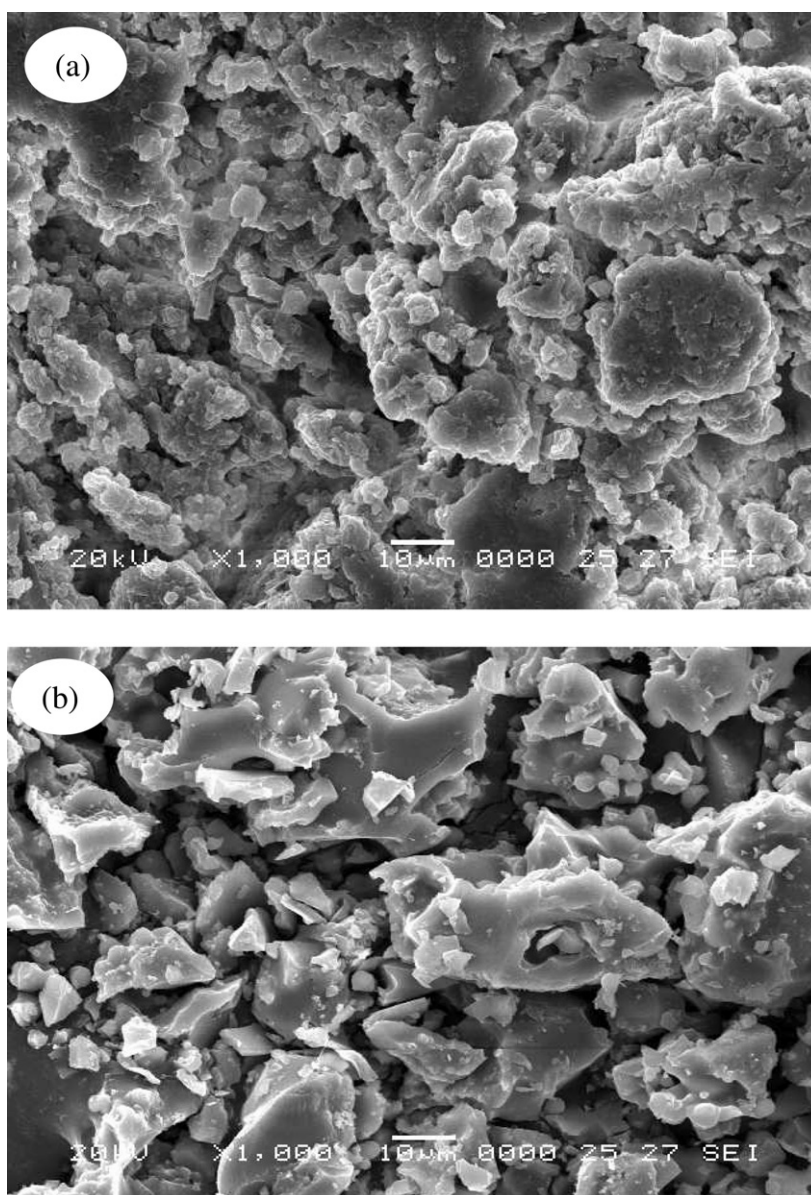


Figure 4. SEM photographs of (a) Cu(II)-PN-him and (b) Cu(II)-PN-his.

other authors [27–29] because of the different methodology and strains assayed. The higher antimicrobial activity of the complexes can be explained by the chelation [30]. The mixed ligand complexes containing hist and his show higher activity than the corresponding him and bim complexes due to the chelating nature of the hist and his ligands (figure 5). Also, the normal cell process may be affected by the formation of a hydrogen bond, through the amino nitrogen with the active centers of cell constituents [31, 32]. However, at this stage it is impossible to find a simple explanation for the

Table 5. Biological activities of 1–12 by disc diffusion method (zone formation in mm).

Complex	<i>S. aureus</i>	<i>K. species</i>	<i>P. species</i>	<i>E. coli</i>	<i>P. aeruginosa</i>	<i>A. niger</i>	<i>C. species</i>
Control	20.3	11.3	9.8	16.5	11.8	19.5	19.3
Cu(II)–PN–him	–	12.8	10.6	11.6	–	15.6	16.5
Cu(II)–PN–bim	14.1	14.0	–	14.3	–	–	12.4
Cu(II)–PN–hist	15.2	–	–	15.6	–	16.2	15.2
Cu(II)–PN–his	–	14.5	–	–	–	14.3	–
Ni(II)–PN–him	18.8	19.1	11.1	19.2	12.5	17.3	18.0
Ni(II)–PN–bim	12.4	–	–	12.6	–	14.5	13.5
Ni(II)–PN–hist	18.6	16.7	–	16.8	–	15.6	15.2
Ni(II)–PN–his	18.2	17.7	–	17.3	–	16.2	14.5
Zn(II)–PN–him	19.3	19.0	–	14.5	13.9	17.5	16.5
Zn(II)–PN–bim	14.2	–	–	–	–	17.9	–
Zn(II)–PN–hist	15.8	20.7	–	18.0	–	–	17.6
Zn(II)–PN–his	13.8	17.6	–	18.9	–	–	18.8

–, less active.

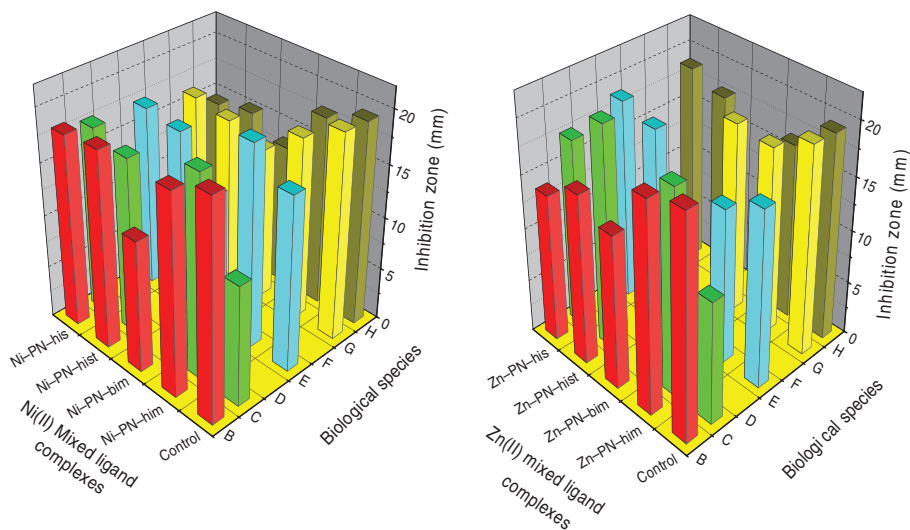


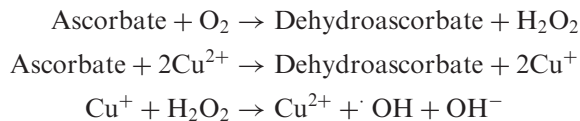
Figure 5. Biological activities of Ni(II) and Zn(II) complexes (zone formation in mm; error limit is ± 1 mm). B – *Staphylococcus aureus*, C – *Klebsiella species*, D – *Proteus species*, E – *Escherichia coli*, F – *Pseudomonas aeruginosa species*, G – *Aspergillus species*, H – *Candida species*.

antimicrobial effect of metal complexes, and further studies will be needed to elucidate this phenomenon.

3.9. DNA cleavage properties

The hydrolytic cleavage of CT DNA in 50 mmol L^{-1} Tris-HCl/ 50 mmol L^{-1} NaCl buffer (pH 7.2) by all the complexes ($5 \mu\text{L}$) in the presence of oxidizing agent (hydrogen peroxide $4 \mu\text{L}$) has been studied by gel electrophoresis (figure S5(a)).

Control experiments (lane 1) using DNA alone and **1–4** and **9–12** in the presence of hydrogen peroxide do not show any apparent cleavage of CT DNA. The octahedral Ni(II) complexes have cleavage activity due to their groove binding nature. Nuclease activities of copper complexes are in contrast with the reported studies [33–35]. This may be due to different methodology and geometry of the complexes. In the presence of ascorbic acid (7 mmol L^{-1}) as a reducing agent in 50 mmol Tris-HCl , 18 mmol NaCl buffer (pH 7.2), **1–4** ($300 \mu\text{mol L}^{-1}$) show chemical nuclease activity (figure S5(b)). A possible course of events is as follows:



Ascorbate will readily reduce cupric ions at higher concentrations than used in these reactions. Cuprous ions react with hydrogen peroxide to produce hydroxyl radicals analogously to Fenton's reagent. Under this condition, cupric ions alone or hydrogen peroxide alone did not give rise to DNA cleavage, although together there was a very slow cleavage probably due to H_2O_2 acting as a reducing agent to convert Cu^{2+} to Cu^+ with the release of O_2 as well as its more usual oxidizing role.

4. Conclusions

The results obtained suggest that PN is a uninegative bidentate ligand, coordinated to metal through deprotonated phenolic oxygen and the oxygen of hydroxymethyl at carbon four. A tetrahedral geometry is assigned for Cu(II)/Zn(II)–PN–him/bim/hist complexes and octahedral for Ni(II)–PN–him/bim/hist complexes. Complexes containing his as one of the ligands have octahedral geometry. High thermal stability of the complexes indicates a strong metal–ligand bond. The copper complexes possess irreversible redox properties. The *in vitro* antimicrobial studies indicate complexes containing hist and his show higher activity than the corresponding him and bim complexes. Nickel complexes exhibit nuclease activity in the presence of H_2O_2 ; copper complexes exhibit nuclease activity only in the presence of a mixture of ascorbic acid and H_2O_2 .

Supplementary material

Structure of ligands and metal complexes, UV spectra, TGA, and decomposition pattern (scheme), the agrose gel electrophoretic pattern and cyclic voltammetric data of free ligand, binary, and Cu(II) complexes are included in the supplementary materials.

Acknowledgements

The authors M.A. Neelakantan, M. Sundaram, and S. Thalamuthu express sincere thanks to the Management, Director and Principal, National Engineering College, Kovilpatti for constant encouragement.

References

- [1] O. Midttun, S. Hustad, J. Schneede, S.E. Vollset, P.M. Ueland. *Am. J. Clin. Nutr.*, **86**, 131 (2007).
- [2] J.J. Vermeersch, S.C. Franck, L.V. Karabashyan, S. Fermandjian, G. Mirambeau, P.A.D. Garabedian. *Nucleic Acids Res.*, **32**, 5649 (2004).
- [3] J.W.H. Yong, L. Ge, Y.F. Ng, S.N. Tan. *Molecules*, **14**, 5144 (2009).
- [4] R. Percudani, A. Peracchi. *EMBO Rep.*, **4**, 850 (2003).
- [5] A.C. Eliot, J.F. Kirsch. *Annu. Rev. Biochem.*, **73**, 383 (2004).
- [6] N.G. Furmanova, Zh. I. Berdalieva, T.S. Chernaya, V.F. Resnyanskiĭ, N.K. Shiitieva, K.S. Sulaĭmankulov. *Crystallogr. Rep.*, **54**, 228 (2009).
- [7] S. Athimoolam, S. Natarajan. *Acta Crystallogr., Sect. E*, **63**, 2916 (2007).
- [8] J.S. Casas, A. Castineiras, F. Condori, M.D. Couce, U. Russo, A. Sanchez, J. Sordo, J.M. Varela. *Polyhedron*, **19**, 813 (2000).
- [9] J.S. Casas, A. Castineiras, F. Condori, M.D. Couce, U. Russo, A. Sanchez, J. Sordo, J.M. Varela, E.M.V. Lopez. *J. Organomet. Chem.*, **689**, 620 (2004).
- [10] M.S.E. Ezaby, M. Rashad, N.M. Moussa. *J. Inorg. Nucl. Chem.*, **39**, 175 (1977).
- [11] D.F. Back, G.M.D. Oliveira, E.S. Lang. *J. Inorg. Biochem.*, **100**, 1698 (2006).
- [12] D.D. Perrin, W.L.F. Armarego, D.R. Perrin. *Purification of Laboratory Chemicals*, Pergamon Press, Oxford (1980).
- [13] M.J. Pelczar, E.C.S. Chan, N.R. Krieg. *Microbiology*, 5th Edn, Blackwell Science, New York (1998).
- [14] W.J. Geary. *Coord. Chem. Rev.*, **7**, 81 (1971).
- [15] A.A. Soliman, G.G. Mohamed. *Thermochim. Acta*, **421**, 151 (2004).
- [16] A.A. Soliman, W. Linert. *Thermochim. Acta*, **338**, 67 (1999).
- [17] K. Nakamoto. *Infrared and Raman Spectra of Inorganic and Coordination Compounds*, 4th Edn, Wiley-Interscience, New York, Chichester, Brisbane (1986).
- [18] K. Yang, L. Wang, J. Wu, Z. Yang, X. Gao. *J. Inorg. Biochem.*, **52**, 151 (1993).
- [19] A.B.P. Lever. *Inorganic Electronic Spectroscopy*, Elsevier, New York (1971).
- [20] S.A. Sallam, A.S. Orabi, B.A. El-Shetary, A. Lentz. *Transition Met. Chem.*, **27**, 447 (2002).
- [21] M. Massacesi, D.G. Ponticelli, V.B. Addepalli, V.G. Krishnan. *J. Mol. Struct.*, **48**, 55 (1978).
- [22] M. Massacesi, D.G. Ponticelli, V.B. Addepalli, V.G. Krishnan. *J. Mol. Struct.*, **51**, 27 (1979).
- [23] S. Hedewy, S.K.K. Hoffman, M.S. Masoud, J. Goslar. *Spectrosc. Lett.*, **19**, 917 (1986).
- [24] B.A. Goodman, J.B. Raynor. *Adv. Inorg. Chem. RadioChem.*, **13**, 135 (1970).
- [25] R. Klement, F. Stock, H. Elias, H. Paulus, P. Pelikan, M. Valko, M. Mazur. *Polyhedron*, **18**, 3617 (1999).
- [26] A.M. Bond, K.B. Oldham, G.A. Snook. *Anal. Chem.*, **72**, 3492 (2000).
- [27] M.S. Nair, S. Regupathy. *J. Coord. Chem.*, **63**, 361 (2010).
- [28] S. Budagumpi, U. Shetti, N.V. Kulkarni, V.K. Revankar. *J. Coord. Chem.*, **62**, 3961 (2009).
- [29] G.B. Bagihalli, S.A. Patil. *J. Coord. Chem.*, **62**, 1690 (2009).
- [30] B.G. Tweedy. *Phytopathology*, **55**, 910 (1964).
- [31] N. Dharmaraj, P. Viswanathamurthi, K. Natarajan. *Transition Met. Chem.*, **26**, 105 (2001).
- [32] M.A. Neelakantan, F. Rusalraj, J. Dharmaraja, S. Johnsonraja, T. Jeyakumar, M.S. Pillai. *Spectrochim. Acta*, **71A**, 1599 (2008).
- [33] J. Sun, S.Y. Deng, L. Zhang, J. He, L. Jiang, Z.W. Mao, L.N. Ji. *J. Coord. Chem.*, **62**, 3284 (2009).
- [34] N. Raman, A. Sakthivel, K. Rajasekaran. *J. Coord. Chem.*, **62**, 1661 (2009).
- [35] K.M. Ibrahim, I.M. Gabr, R.R. Zaky. *J. Coord. Chem.*, **62**, 1100 (2009).